LITHOS 492–493 (2025) 107864

Contents lists available at ScienceDirect

LITHOS

journal homepage: www.elsevier.com/locate/lithos

Temporal variation in oxygen isotopes of peraluminous granites derived from sedimentary sources

Claire E. Bucholz *, Juan D. Hernández-Montenegro

California Institute of Technology, Pasadena, CA 91125, USA

ARTICLE INFO

Keywords:
Granite
Peraluminous
Oxygen isotopes
Weathering
Clay

ABSTRACT

The oxygen isotopic composition of magmatic rocks provides critical constraints on the contributions of crust versus mantle in their genesis. Peraluminous granites derived from partial melting of sedimentary rocks offer a unique archive to examine how the oxygen isotope composition of sedimentary rocks recycled into magmas has changed throughout Earth history. In this study, we explore this record through a two-pronged approach. First, we compile a comprehensive dataset of oxygen isotope bulk-rock and mineral analyses from globally distributed peraluminous granites and volcanic rocks ranging in age from 3.2 billion years to 6 million years. Second, we model the isotopic fractionation between sedimentary source rocks and derivative melts, as well as minerals in equilibrium with the melt during anatexis. Our compilation demonstrates a progressive increase in $\delta^{18}O$ values of zircon and garnet from the Archean to Paleoproterozoic and again in the latest Neoproterozoic to Phanerozoic. Specifically, the average $\delta^{18}O$ of zircon from peraluminous granites increases from 6.7 ± 1.0 ‰ to 9.5 ± 0.8 ‰ at ~ 2.35 Ga, followed by another increase to 10.4 ± 0.7 ‰ after 600 Ma (errors are ± 1 s.d.). These observations align with the sedimentary rock record which suggests enhanced weathering and clay deposition resulting from tectonic and biological forcings. Furthermore, the increase in $\delta^{18}O$ of peraluminous granites broadly mirrors similar secular increases in the $\delta^{18}O$ values of siliciclastic sedimentary rocks. However, using our modeled fractionations between melt and source rock, the reconstructed source-rock $\delta^{18}O$ values capture only the lower end of the siliciclastic sedimentary rock range, suggesting that sedimentary rocks recycled into magmas have, on average, lower $\delta^{18}O$ values than coeval clay-rich shales. We propose that any global analyses of oxygen isotopes in magmatic rocks or zircon should use the average values of calculated source rocks for peraluminous granites in defining crustal contributions. Furthermore, our study highlights the broader implications of the observed trends, including the progressive contamination of the mantle and elevation of its $\delta^{18}O$ values.

1. Introduction

Oxygen isotope ratios (denoted as $\delta^{18}O$; where $\delta^{18}O = ([^{18}O/^{16}O]_{sample}/[^{18}O/^{16}O]_{VSMOW} - 1)*1000$ ‰)) are a longstanding tool for quantifying the relative contributions of crust and mantle to magmas (Taylor, 1968). Basaltic glasses from "normal" (unenriched) mid-ocean ridges (N-MORB), representing products of partial melting of the depleted upper mantle with only minimal recycled crust, have $\delta^{18}O$ values of ~ 5.6 ± 0.2 ‰ (Eiler et al., 2000). Fractional crystallization of a basalt to a granitic melt with ~70 wt% SiO_2 (at less than ~15 % melt fraction remaining) results in an increase in melt $\delta^{18}O$ by 1–1.5 ‰ (Bucholz et al., 2017 and references therein). Consequently, melts derived from the unenriched mantle which subsequently differentiate will have $\delta^{18}O$ < ~7 ‰. In contrast, magmatic rocks that have assimilated (or are derived from) crustal rocks that have interacted with meteoric or marine waters can deviate both positively and negatively from these values.

Although bulk igneous rocks were initially analyzed for oxygen isotopes, minerals have been the analyte of choice for the last two to three decades because certain phases, such as olivine in mafic rocks and zircon in felsic rocks, exhibit greater resistance to both subsolidus diffusive resetting and alteration of magmatic $\delta^{18}O$ values. In particular, the zircon $\delta^{18}O$ record has been extensively employed to investigate the assimilation of sedimentary materials into felsic magmas and thus crustal recycling over time (e.g., Valley et al., 2005; Wilde et al., 2001). However, the detrital zircon record (Fig. 1) comes with certain limitations. Foremost among these is the detachment of detrital zircon from any information about their source rock. Although trace elements in

* Corresponding author.
E-mail address: cbucholz@caltech.edu (C.E. Bucholz).

https://doi.org/10.1016/j.lithos.2024.107864
Received 17 June 2024; Received in revised form 29 October 2024; Accepted 5 November 2024
Available online 12 November 2024

zircon can serve as proxies for source rock composition (Grimes et al., 2015), concerns have been raised about applying proxies based on zircon from Phanerozoic granites to older samples (e.g., Bucholz et al., 2022; Roberts et al., 2024). Another limitation is the potential bias in the detrital record towards more easily eroded upper crustal lithologies (Spencer et al., 2022). Similarly, compilations of zircon data from magmatic rocks can be skewed due to overrepresent a particular locality at any given time (Sundell et al., 2024).

When quantifying the amount of crustal versus mantle contribution to magmas the selection of mantle and crustal end members becomes crucial and difficult to do with large datasets covering disparate localities. While the unenriched mantle is generally presumed to have remained relatively constant throughout Earth's history, the weathered crustal end-member likely varied greatly due to changes in weathering regimes, shifts in the $\delta^{18}O$ of meteoric and marine waters, or changes in surface temperature. One potential way to address this question is to look at oxygen isotopes of siliciclastic sedimentary rocks (Bindeman et al., 2016; Bindeman et al., 2018; Payne et al., 2015), which represent an important component of crustal lithologies that are assimilated by magmas. However, this record, albeit informative, displays significant variability (~10 ‰ in $\delta^{18}O$ at any given time; Fig. 1), and does not conclusively contribute to our understanding of what is being incorporated into magmas during assimilation. In short, many researchers have focused primarily either on the detrital zircon or the siliciclastic sedimentary record but have not closed the loop by interrogating the felsic igneous record linking the two.

The oxygen isotopic composition of granites that are the products of melting of sedimentary rocks is a more direct approach to discern the effect of crustal assimilation on oxygen isotope ratios of magmas. Although commonly referred to as "S-type" granites, indicating their formation from melting of (meta-)sedimentary rocks, the original definition of S-type granites had much more specific geochemical criteria including, for example, Na_2O and K_2O contents (Chappell and White, 1974). Here, we opt to refer to them as peraluminous granites as a more general geochemical classification (with a bulk-rock aluminum saturation index (ASI = molar oxide $Al_2O_3/(CaO + Na_2O + K_2O)$] greater than 1, Bonin et al., 2020; Bucholz, 2025). It is important to note that not all peraluminous granites originate from partial melting of metasedimentary rocks; for example, some form through differentiation of metaluminous (ASI < 1) melts. However, when we refer to peraluminous granites in this paper, we are specifically indicating those that have been suggested to have sedimentary sources, based on field, petrologic, and geochemical evidence.

Peraluminous granites derived from sedimentary sources exhibit $\delta^{18}O$ values elevated above those derived from differentiation of mantle-derived basalts (e.g., as first pointed out by O'Neil et al., 1977; O'Neil and Chappell, 1977). However, whether their $\delta^{18}O$ has varied through time has not been comprehensively explored. Notably, studies examining oxygen isotopes in peraluminous granites around the Archean-Proterozoic transition have been conducted (Bucholz and Spencer, 2019; Liebmann et al., 2021a; Liebmann et al., 2021b; Lu et al., 2021; Xie et al., 2022). These studies found an increase of ~3 ‰ in zircon $\delta^{18}O$ from peraluminous granites at c. 2.35 Ga, correlated with similar increases observed in the detrital and igneous zircon record (e.g., Spencer et al., 2019; Valley et al., 2005) and shale record (Bindeman et al., 2016; Bindeman et al., 2018), possibly related to enhanced weathering coincident with emergence of large continental landmasses in the Neoarchean to Paleoproteroizc, as well as the Great Oxidation Event. However, despite evidence from the sedimentary record indicating dynamic changes in surface weathering and sediment deposition during the Neoproterozoic to Phanerozoic (e.g., Bayon et al., 2022; Campbell and Squire, 2010; Husson and Peters, 2017; Kennedy et al., 2006; McMahon and Davies, 2018), a comparable assessment of oxygen isotopes for younger peraluminous granites remains unexplored.

Here, we address this knowledge gap by building upon previous studies of oxygen isotopes in peraluminous granites in the following ways. First, we present a new compilation of oxygen isotope data (both of bulk-rock and minerals) from Mesoarchean to Miocene strongly peraluminous granites and felsic volcanic rocks. Second, we present results of thermodynamic modeling of partial melting of siliciclastic sedimentary rocks coupled with oxygen isotopic fractionation to predict the difference in oxygen isotopes between the source rock and derivative granite melts. Finally, we integrate and reconcile our new data compilation and modeling results with existing knowledge of the sedimentary rock record, achieving a global understanding of how changes in the Earth's surface environment have directly impacted the magmatic oxygen isotope record.

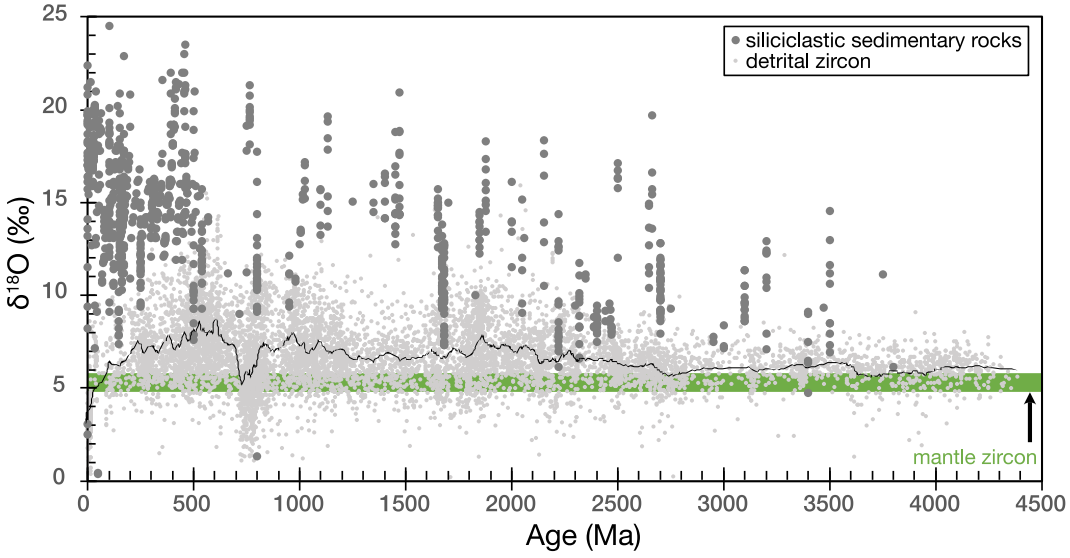

Fig. 1. Oxygen isotopes in siliciclastic sedimentary rocks and detrital zircon versus age. Siliciclastic sedimentary rock analyses are those compiled in Payne et al. (2015) and Bindeman et al. (2016, 2018). The detrital zircon compilation is from Spencer et al. (2022) shown with a moving average of every 100 data points. The envelope of "mantle" zircon value of 5.3 ± 0.6 ‰ is from Page et al. (2007) and Cavosie et al. (2009).

2. Methods

2.1. Data compilation

We compiled the oxygen isotope analyses of bulk-rock and minerals (zircon, garnet, and quartz) from peraluminous granitoids and rhyolites/dacites. These plutonic and volcanic rocks were previously identified by researchers as having siliciclastic metasedimentary source rocks, such as metapelites and metapsammites. The basis for these conclusions involved a variable combination of field observations, petrography, major and trace element data, radiogenic and stable isotopic data, and examination of magmatic and inherited zircon populations. A similar compilation approach was taken by Bucholz (2022) and interested readers are referred to that publication for further details on identification of granites derived through the partial melting of sedimentary rocks. If the original studies of a peraluminous granite indicated a mantle-component in a sample's origin (i.e., it was not derived from a purely sedimentary source), based on either field relationships suggesting consanguinity with mafic rocks (e.g., the presence of mafic enclaves or mingling textures between granitic and mafic rocks) or radiogenic isotopes, we did not include these samples in our subsequent analysis. For completeness, however, we do include the data from these samples in the compilation (see Tables S1, S2, Fig. S1).

Bulk-rock analyses were available for 68 % of samples with oxygen isotope data. Among the samples with bulk-rock data, the majority are strongly peraluminous (72 %, ASI > 1.1), while the remainder are mildly peraluminous (ASI = 1–1.1). When bulk-rock analyses were not available, we relied on the presence of peraluminous indicator minerals (such as muscovite, garnet, or tourmaline) and the descriptions of the original study authors indicating derivation from sedimentary sources. Samples were not filtered based on bulk-rock data beyond the classification of being peraluminous because our analysis primarily relies of zircon and garnet (and to a lesser extent quartz) oxygen isotope data, which are deemed more reliable to bulk-rock values and less susceptible to post-crystallization alteration.

In the compiled data, oxygen isotopes were analyzed by different methods depending on the publication date of the original study and the material analyzed. Studies predating the advent of isotopic analysis in minerals via secondary ion mass spectrometry (SIMS) in the 1990s (Eiler et al., 1997; Valley and Graham, 1991) exclusively used fluorination methods either involving conventional fluorination methods using most commonly BrF_5, but also ClF_3 and F_2 (Clayton and Mayeda, 1963) or laser fluorination (Sharp, 1990) for bulk-rock powders and mineral separates. With the establishment of high-precision analysis of oxygen isotope ratios in zircon (and garnet) using large geometry SIMS instruments (e.g., Kita et al., 2009; Mojzsis et al., 2001; Wilde et al., 2001), subsequent studies on granites predominantly prioritized zircon analysis via SIMS, which continues to the present day. This preference stems from the general resistance of zircon to alteration in comparison to other phases (with some exceptions, see below), its abundance in silicic samples, and the convenience of obtaining comprehensive information on a single phase (including U-Th-Pb ages, trace elements, and Hf isotopes). Nevertheless, fluorination methods continue to be utilized to determine oxygen isotope ratios of major phases (and occasionally zircon) and bulk-rock powders. Although zircon and garnet are the preferred archive for interrogating oxygen isotope ratios in peraluminous granites due to their resistance to alteration and slow intracrystalline oxygen diffusivities, our compilation also includes bulk-rock and quartz values for comparative purposes. This decision was based on the relatively limited availability of oxygen isotope data specifically for peraluminous granites and to generate a comprehensive dataset.

Although SIMS analysis of oxygen isotope ratios in silicates, particularly zircon, is now relatively routine, care must be taken during analysis, particularly in attention to reference material selection, analysis protocols, as well as sample surface topography and geometry (Kita et al., 2011, Kita et al., 2009; see review of Liebmann et al., 2023). In the context of peraluminous granites, it is crucial to distinguish between magmatic rims and inherited cores to obtain magmatic oxygen isotope compositions. In the compiled datasets SIMS analyses of multiple zircon (or in some instances garnet) were undertaken per sample, careful attention was paid to any metadata provided by the authors and used in deciding which data to include or exclude. For example, any analyses identified as inherited or xenocrystic (either texturally or by older U—Pb ages analyzed on the same zircon spots) were excluded. Most of zircon analyses were conducted via SIMS, however two studies utilized laser fluorination to analyze bulk zircon aliquots (Gao et al., 2014; Wu et al., 2006). In this case, we included the data for completeness although inherited zircon cores were likely analyzed in these studies. Second, although only an extremely small percent of zircon SIMS data included in this compilation had $^{16}OH/^{16}O$ ratios analyzed simultaneously with $^{18}O/^{16}O$ ratios (~6 % of all analyses), when this data was available it was used as a screening tool for samples potentially affected by radiation damage, water incorporation into the zircon crystal lattice, and alteration of primary oxygen isotope ratios (e.g., Liebmann et al., 2021c Pidgeon et al., 2017; Wang et al., 2014). In cases where this data was available, we followed exclusion recommendations made by the original authors of the studies.

All compiled data including oxygen isotope values, major element analyses for bulk-rocks, geochronology, oxygen isotope analysis method, inferred source rock depositional age, and designated group are given in Supplementary Table S1. Both individual zircon and garnet analyses (Table S2) and calculated sample averages (Table S1) are provided.

2.2. Thermodynamic modeling of isotope fractionation during partial melting

2.2.1. Phase equilibria modeling

Phase equilibrium modeling was used to estimate the proportions and compositions of minerals and melt during partial melting. The calculations were performed using the software Theriak-Domino in the system MnO-Na_2O-K_2O-CaO-FeO-MgO-Al_2O_3-SiO_2-H_2O-TiO_2-O_2 (MnNKCFMASHTO), which is appropriate for partial melting of metasedimentary rocks (White et al., 2014b). The thermodynamic dataset includes the internally consistent database of Holland and Powell (2011) and activity-composition (*a-x*) relations for solid solution phases typically involved in anatexis of metapelites – i.e., biotite (Bt), garnet (Grt), cordierite (Crd), orthopyroxene (Opx), and staurolite (St) (White et al., 2014b), silicate melt (Melt) and white mica (Ms) (White et al., 2014a), ilmenite-hematite (Ilm-Hem) (White et al. (2000)), spinel-magnetite (Spl-Mag) (White et al., 2002), plagioclase (Pl) and K-feldspar (Kfs) (Holland and Powell, 2003), and epidote (Ep) (Holland and Powell, 2011). Pure phases include quartz (Qtz), rutile (Rt), titanite (Ttn), sillimanite (Sil), andalusite (And), kyanite (Ky), and hydrous fluid (H_2O). The mineral abbreviations herein are from Warr (2021).

All calculations were run at fixed pressures of 0.5 and 1.0 GPa and a temperature range of 600–1000 °C, conditions expected to intersect crustal geotherms across Earth history (Holder et al., 2019). Also, partial melting was considered to occur under minimally saturated water conditions (i.e., <0.5 mol% H_2O at the solidus), which avoids unconstrained overestimation of the melt fraction with fluid-present melting. At each pressure, we performed calculations with oxygen fugacity buffered at FMQ+2, FMQ, and FMQ-2, where FMQ corresponds to the fayalite-magnetite-quartz buffer. Finally, the $Fe^{3+}/\Sigma Fe$ proportion of the melt phase was estimated independently using the equations from Kress and Carmichael (1991) since the *a-x* model for silicate melt has no ferric iron component.

2.2.2. Siliciclastic sedimentary starting compositions

To accurately represent the major element variability observed in silciclastic sedimentary rocks, we selected five starting compositions based on the dataset of pelitic compositions compiled by Forshaw and

Pattison (2023) (Table S3; Fig. S2). This dataset includes 5729 major-element bulk-rock analyses, from which we derived average compositions for distinct SiO_2 ranges: 53–57 wt% (n = 474), 58–62 wt% (n = 1290), 63–67 wt% (n = 1505), 68–72 wt% (n = 766), and 73–77 wt% (n = 295). These ranges are defined to capture a systematic decrease in Al_2O_3, and $FeO_T + MgO + TiO_2$ with increasing SiO_2 due to variations in the proportions of quartz, feldspar and micas in pelites (Fig. S2). Data were normalized to 100 wt% to ensure consistency in comparison and interpretation across the defined SiO_2 ranges.

2.2.3. Modeling of oxygen isotope fractionation during partial melting

We used our results from phase equilibrium modeling to predict fractionation of oxygen isotopes between stable phases during anatexis. First, isotopic fractionation between quartz and any pure phase j was estimated using Eq. 1:

$$1000 \times ln\alpha_{Qtz-j} = \left(\frac{A_{Qtz-j} \times 10^6}{T^2} + \frac{B_{Qtz-j} \times 10^3}{T} + C_{Qtz-j}\right) \quad (1)$$

where $1000 \times ln\alpha_{Qtz-j} \approx \Delta^{18}O_{Qtz-j} = \delta^{18}O_{Qtz} - \delta^{18}O_j$, T is the temperature in Kelvin, and A, B, C are characteristic polynomial parameters describing the partitioning between quartz and phase j taken from the internally-consistent database of Vho et al. (2019).

Coefficients A, B, and C in this database were derived using data from equilibrium experiments, theoretically derived fractionation factors, and semi-empirical bond-strength models. The calibration strategy involved the generation of a secondary dataset across a temperature range of 0–900 °C, which was then used to find the best-fit polynomial parameters through iterative fitting and global optimization using least squares. This approach ensures internal consistency, meaning the derived expressions agree with theoretical definitions and reference values, account for all available data simultaneously, and can reproduce estimates of oxygen isotope fractionation for any mineral pair within the calibration dataset, respecting the stated uncertainties of the underlying data (Vho et al., 2019).

For any solid solution s, the contribution of each endmember k to the total isotopic fractionation between quartz and s is calculated from Eq. 2 as follows:

$$\delta^{18}O_{Qtz} - \delta^{18}O_s \approx \sum_1^k \left(\frac{A_{Qtz-k} \times 10^6}{T^2} + \frac{B_{Qtz-k} \times 10^3}{T} + C_{Qtz-k}\right) * X_{k-s} \times \frac{N_{k-s}}{N_s} \quad (2)$$

where X_{k-s} is the molar fraction of k in s, and N_{k-s} and N_s are the fractions of oxygen in endmember k and in the entire solid solution s, respectively.

Because the a-x model of the silicate melt phase describes it as a molecular mixture of fictive endmembers not included in the oxygen isotope fractionation database, the melt is treated as a solid solution consisting of its normative minerals (see Eiler, 2001 for discussion), with molar fractions corresponding to the normative modal proportion in mol.%. The biotite, cordierite, and staurolite solid solutions are treated as pure phases for calculations of oxygen isotope fractionation since the database does not include several of their thermodynamic endmembers but includes them as single phases. For endmembers of other solid solutions not included in the database, we adopt the A, B, C coefficients of endmembers that are structurally and compositionally similar or average them when the missing endmember could be obtained as a mixture of other two endmember species in the database. A summary of all pure phases and solution endmembers considered and their corresponding A, B, C parameters is given in Table S4.

With $\Delta^{18}O$ values for all stable phases relative to quartz, the $\delta^{18}O$ of each phase can be obtained by assuming mass balance in a closed system, a starting $\delta^{18}O$ for the system, and 'effective oxygen modal proportion' p_{eff} for each phase:

$$p^i_{eff} = \frac{X^i_O \times p^i_{molar}}{\sum_1^n X^n_O \times p^n_{molar}} \quad (3)$$

where X^i_O and p^i_{molar} are the oxygen fraction and molar proportion of phase i, and n is the number of stable phases in the system at each point. The full model is provided as a supplemental code in the Supplemental Material.

3. Results

3.1. Data compilation

The final compiled dataset (not including samples with an inferred mantle contribution) consists of analyses from a total of 632 samples from globally distributed localities (Table 1; Fig. 2, S3-S5), with varying availability of oxygen isotope data for different phases. Zircon, garnet, quartz, and bulk-rock, data were available for 167, 75, 189, and 342 samples, respectively, sometimes with data for more than one phase for an individual sample. A total of 2795 individual zircon SIMS analyses were included in the final compilation. In cases where multiple analyses were conducted for zircon, quartz, and garnet within a single sample, we computed an average value for each phase in a sample. This averaging approach mitigates bias towards any specific sample. Sample garnet and zircon $\delta^{18}O$ averages versus crystallization age are shown in Fig. 3. Sample bulk-rock and quartz $\delta^{18}O$ versus crystallization age are shown in Fig. S3a.

Both a moving average and LOWESS curve (Cleveland, 1979) through the zircon dataset are shown in Fig. 3a and demonstrate a few notable features. First, there is an increase in both the moving average and LOWESS curve in the Paleoproterozoic from ~7 ‰ to ~9 ‰ and eventually up to ~10 ‰ in the Mesoproterozoic (as previously documented for peraluminous granites, e.g., **Liebmann et al., 2021b**). Given the limited size of the dataset, it is unclear whether this transition marks a relatively sharp increase (as observed in the moving average) or rather a progressive increase in maximum values from the Neoarchean to ~ 1.7 Ga (as indicated by the LOWESS curve). Secondly, there is an increase by ~ 1 ‰ in the latest Neoproterozoic into Paleozoic, followed by another decrease by ~ 1 ‰ in samples with ages < 200 Ma.

To gain deeper insight into the variations observed, we categorized the samples based on both their crystallization age and the depositional age of their sedimentary source rocks, following the methodology of Bucholz (2022). The defined groups are as follows: Group 1 (>2355 Ma crystallization age and source rock age), Group 2 (600–2355 Ma crystallization age and > 600 Ma source rock age), Group 3 (<600 Ma crystallization age, <600 Ma source rock age), Group 4 (<600 Ma crystallization age, >600 Ma source rock age), Group 5 (<600 Ma crystallization age, unknown source rock age).

The choice of the Paleoproterozoic age boundary (2355 Ma) is based on the moving average curve (Fig. 3a) and previous observations of shifts in oxygen isotopes of zircon from peraluminous granites and the broader detrital record (Liebmann et al., 2021b; Lu et al., 2021; Spencer et al., 2019; Spencer et al., 2022; Xie et al., 2022). The 600 Ma age boundary, while somewhat arbitrary, was selected primarily due to the increase observed at ~500 Ma in the moving average curve. This boundary allows for ~100 million years of sediment deposition, followed by burial and metamorphism, prior to the crystallization age of the peraluminous granites. It is important to note that any age between 600 and 800 Ma could have served as a suitable boundary, and the results would remain consistent given the lack of samples from this period. Although these boundaries may be somewhat artificial as there is no reason that they must be sharp in nature, they provide a useful framework for discussing the influence of source rock depositional age on the $\delta^{18}O$ values of peraluminous granites.

A summary of statistics of zircon, garnet, quartz, and bulk-rock $\delta^{18}O$ values for each group are given in Table 1. The grand mean of sample

Table 1
Summary of average* $\delta^{18}O$ for samples from Groups 1–5.

			ZIRCON			GARNET			QUARTZ			BULK-ROCK		
Group	Crystallization Age	Source Rock Depositional Age	n*	$\delta^{18}O$ (‰)	s.d.	n*	$\delta^{18}O$ (‰)	s.d.	n*	$\delta^{18}O$ (‰)	s.d.	n*	$\delta^{18}O$ (‰)	s.d.
1	>2355 Ma	>2355 Ma	13	6.71	*0.98*	17	6.48	*1.10*	7	9.37	0.71	66	9.80	1.44
2	600–2355 Ma	600–2355 Ma	58	9.49	*0.75*	37	10.17	*0.94*	82	13.23	0.89	76	11.38	1.54
3	<600 Ma	600–2355 Ma	66	10.44	*0.71*	12	10.86	*0.62*	52	13.01	0.97	137	12.82	1.86
4	<600 Ma	<600 Ma	23	9.06	*0.84*	2	9.20	*0.00*	38	12.50	1.02	45	11.34	1.05
5	<600 Ma	unknown	7	9.90	*0.78*	7	10.27	*0.10*	10	13.01	1.00	18	12.77	1.47

n* = number of samples included in average.
In calculation of these averages, we did not use a weighted average considering uncertainties because of both SIMS and fluorination data used in the compilation. A sample average based on many SIMS analyses of individual grains will typically have a standard deviation on the order of > 0.5‰. In contrast, an analysis via fluorination also involves sampling many grains (however, now as one aliquot), but the reported uncertainty, which represents analytical uncertainty, is much smaller (typically ~ 0.1 to 0.2‰, 2 s.d.). In sum, errors associated with samples measured via SIMS are capturing sample variability, while the error associated with fluorination represent analytical error, and thus are not directly comparable.

Fig. 2. Global distribution of peraluminous granite localities with oxygen isotope data included in the compilation. Type of data from each locality including group and type of material analyzed is indicated by colour and size/shape of symbol, respectively. For clarification on classification by Groups, see Section 3.1.

average zircon $\delta^{18}O$ from Groups 1, 2, 3, and 4 are 6.71 ± 0.98 ‰, 9.49 ± 0.75 ‰, 10.44 ± 0.71 ‰, and 9.06 ± 0.84 ‰ (1σ) and medians are 6.45 ‰, 9.44 ‰, 10.36 ‰, 9.04 ‰ (Figs. 3, 4a). When individual zircon analyses (instead of sample averages) are considered, a similar difference among groups are observed (Fig. 4b). The average of individual zircon $\delta^{18}O$ from Groups 1, 2, 3, and 4 are 7.08 ± 1.10 ‰, 9.56 ± 1.14 ‰, 10.53 ± 0.93 ‰, and 9.18 ± 1.03 ‰ and medians are 7.00 ‰, 9.49 ‰, 10.60 ‰, and 9.19 ‰, respectively (Fig. 4b). Notably, the decrease in zircon $\delta^{18}O$ in samples < 200 Ma (Fig. 3a) are all ascribed to Group 4 samples with > 600 Ma source rock depositional ages (Fig. 3b).

Garnet data is more limited, but $\delta^{18}O$ values of garnet increase the same order of magnitude as zircon. Averages for Groups 1–3 are 6.48 ± 1.10 ‰, 10.17 ± 0.94 ‰, and 10.86 ± 0.62 ‰ (1σ.) (Only 2 samples have garnet analyses from Group 4, precluding a meaningful average.) Quartz $\delta^{18}O$ increases from Group 1 to Group 2 with averages of 9.37 ± 0.71 and 13.23 ± 0.89 ‰ (1σ). Group 3 and 4 average quartz $\delta^{18}O$ are indistinguishable from Group 2, 13.01 ± 0.97, and 12.50 ± 1.02 ‰ (Fig. S3b). Average bulk-rock $\delta^{18}O$ values for Groups 1–4 are 9.80 ± 1.44, 11.38 ± 1.54, 12.82 ± 1.86, and 11.34 ± 1.05 ‰ (1σ; Fig. S3c).

3.2. Model results

Full model results including phase diagrams for all modeled bulk compositions at different pressures and oxygen fugacities are shown in Fig. S6 and S7. Representative model results for the intermediate-low SiO_2 starting composition (SiO_2 = 58–63 wt%) at 0.5 GPa and 1.0 GPa and FMQ-2 are shown in Fig. 5. The low oxygen fugacity is typical for sedimentary-derived peraluminous granites across Earth history due to the presence of reduced phases such as graphite in their sedimentary sources (Bucholz et al., 2018; Whalen and Chappell, 1988).

Fractionation of oxygen isotopes between the original bulk-rock source composition and that of an anatectic melt ($\Delta_{melt\text{-}source}$) is not strongly affected by variations in oxygen fugacity or pressure (with $\Delta_{melt\text{-}source}$ varying typically by <0.1 ‰ at a fixed temperature and bulk-composition; Fig. 5b,e, S8). However, there are subtle effects. For example, increasing pressure at a fixed temperature and oxygen fugacity results in greater stability of garnet, relative to plagioclase, resulting in larger fractionations (by 0–0.2 ‰) at 1.0 versus 0.5 GPa due to garnet being relatively isotopically light (Fig. 5b,e, S8).

In contrast, the most pronounced control of fractionation between the source and the anatectic melt is the source-rock silica contents. As the modal proportion of quartz increases among the stable mineral

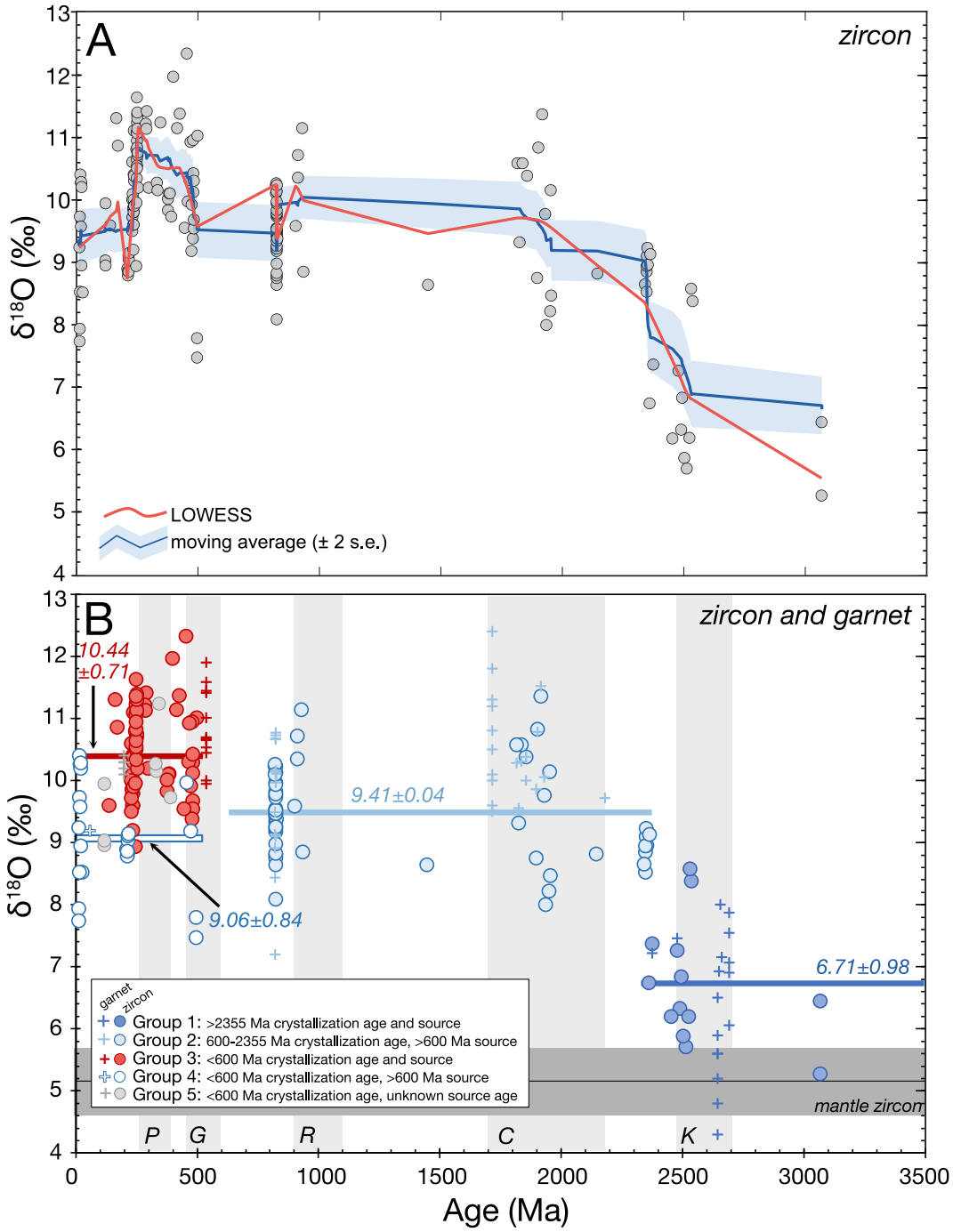

Fig. 3. Oxygen isotope data from peraluminous granites versus crystallization age. Individual data points indicate sample averages. Errors on average not shown, but the average two standard deviation on averages of analyses from individual samples is 1.1 ‰ (see Table S1). [Note, data from mantle-hosted peraluminous granites from the Oman ophiolite (Spencer et al., 2017) are not shown to focus on peraluminous granites formed from sedimentary rocks more typical of those found in collisional orogens or in back-arc settings.] Similarly, localities inferred to have a mantle component are omitted for clarity but are shown in Fig. S1. (A) Sample average zircon $\delta^{18}O$ is shown without time binning. Blue line and blue shaded region indicate moving average of entire dataset with a 10-sample window size and corresponding 2 s.d. Red line is a LOWESS curve (**Cleveland,** 1979) using a smoothing parameter of 0.15. (B) Zircon and garnet data colored by their classification into groups. Thick horizontal bars of different colors represent average zircon $\delta^{18}O$ values of samples in Groups 1 through 4, with average values (±2 s.d.) indicated. Average zircon values from mantle-derived rocks (plagiogranites and kimberlites) shown in grey bar (5.3 ± 0.6 ‰; Cavosie et al., 2009; Page et al., 2007). Grey vertical bars show times of supercontinent assemblies with capital letters indicating supercontinents; K: Kenorland, C: Columbia, R: Rodinia, G: Gondwana, and P: Pangea. (For interpretation of the references to colour in this figure legend, the reader is referred to the web version of this article.)

assemblages, the fractionation between the melt and the residue decreases (Fig. 5b). For example, at 800 °C, 0.5 GPa, and FMQ-2, partial melting of a source rock with ~55 wt% (low silica and less quartz) results in $\Delta_{melt\text{-}source}$ of ~ + 0.7 ‰, whereas a source with higher SiO_2 ~ 70 wt% (high-intermediate silica, more quartz) yields $\Delta_{melt\text{-}source}$ of ~ − 0.2 ‰. This trend persists for models at different pressure, temperature, and oxygen fugacity conditions (Fig. S8). It is also noteworthy that the extent of fractionation between the melt and the source at different temperatures decreases with increasing SiO_2 of the source, resulting from the source and the residue being largely dominated by quartz for

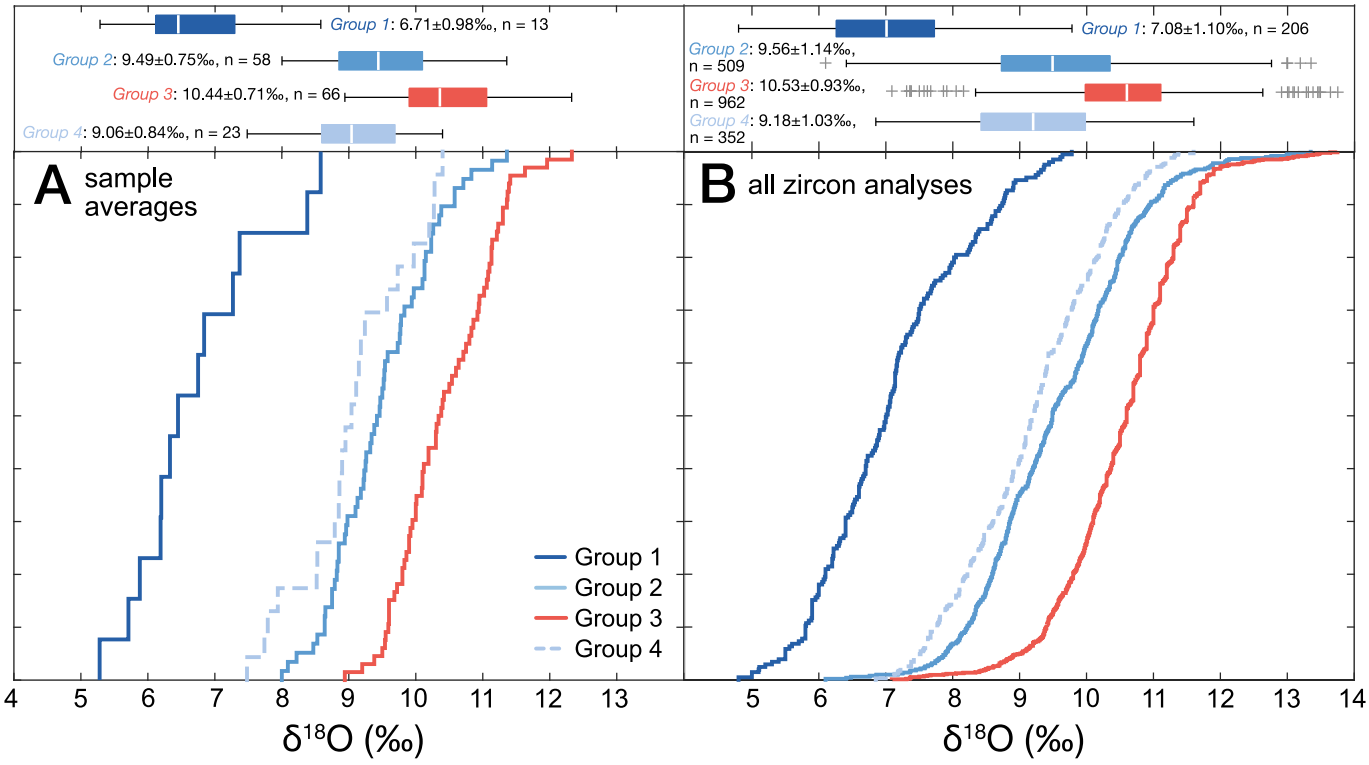

Fig. 4. Summary of compiled zircon data by group. In (a) and (b) sample average zircon analyses and all individual zircon analyses are shown, respectively. Upper panels show box and whisker plots (medians, quartiles, and outliers) for different groups as well as averages (in black text) and number of analyses included (n).

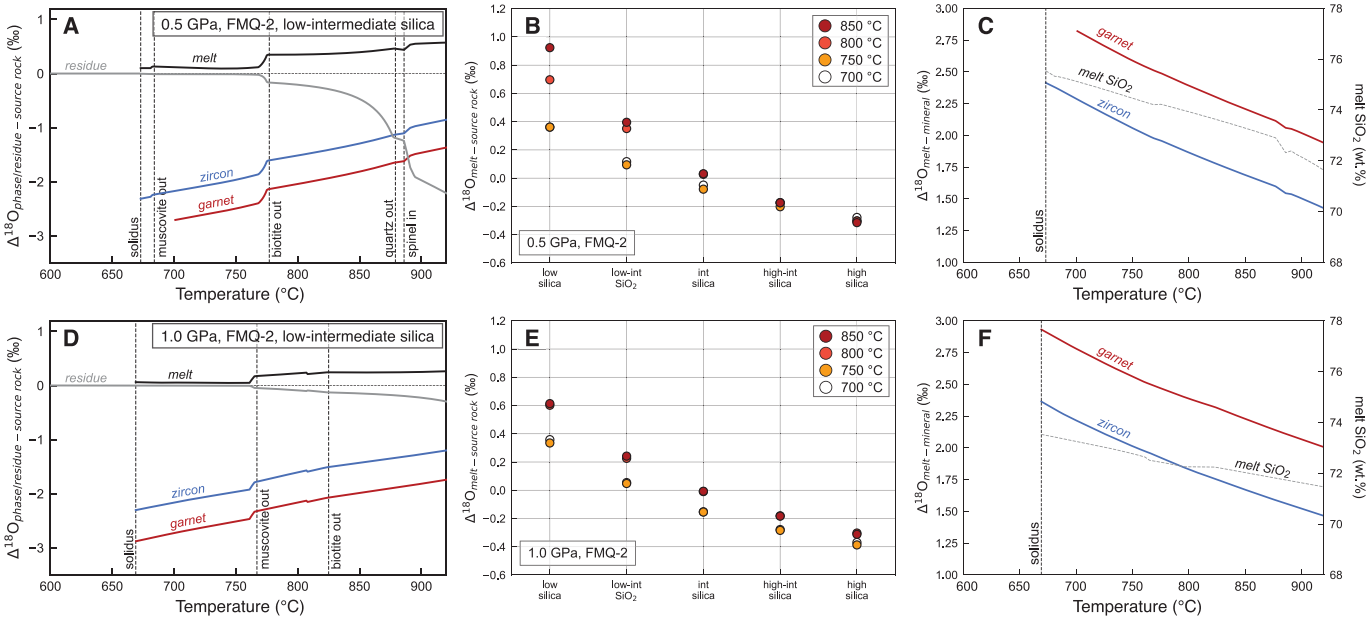

Fig. 5. Summary of model results for the low-intermediate silica sedimentary composition at FMQ-2. (A,D) per mil fractionation between melt, zircon, garnet, and residue versus original source rock as a function of temperature for melting of the low-intermediate silica metasedimentary composition. (B,E) per mil fractionation between melt and source rock for different sedimentary source rock compositions and temperatures (C,F) per mil fractionation between melt and garnet or zircon versus temperature. Modeled melt SiO_2 (normalized on an anhydrous basis) is also shown for reference as a dashed grey line. A, B, and C are models at 0.5 GPa, and D, E, and F for models at 1 GPa.

higher SiO_2 contents. Nonetheless, the absolute values of fractionations between source rock and melt for all modeled conditions are relatively small (<1 ‰) due to the high temperatures of the melting and the relative abundance of quartz and feldspar in both the source rock and the normative composition of the melt. This implies that for a modeling scenario considering partial melting with periodic melt extraction, only minor differences with batch melting are expected as melt loss would have a minimal impact on the isotopic composition of the system.

Thus, in an idealized scenario (i.e., ignoring entrainment of restitic material or disequilibrium melting), if a low to intermediate silica pelitic

rock with a bulk $\delta^{18}O$ of 10 ‰ partially melts at 0.5 GPa and FMQ-2 between 700 and 850 °C, the anatectic melt will have a value of 10–11 ‰ (depending on the bulk-rock composition). Zircon and garnet in equilibrium with a granitic melt will be 2.3–1.8 ‰ and 2.8–2.4 ‰ lower over a temperature range of 700–800 °C (Fig. 5c,f). Therefore, zircon and garnet that subsequently crystallize from this melt over a temperature range of 700–800 °C will have $\delta^{18}O$ values of 7.7–9.2 ‰ and 7.2–8.6 ‰. Thus, magmatic zircon and garnet from peraluminous granites will be ~0.8–2.3 ‰ and 1.4–2.8 ‰ lower than the sedimentary source rock $\delta^{18}O$, respectively.

4. Discussion

4.1. Preservation of magmatic oxygen isotope values in zircon and garnet from peraluminous granites

Oxygen isotope values in zircon and garnet are commonly considered representative of their values at the time of initial mineral growth due to the slow intracrystalline diffusion rates of oxygen in these minerals and their relative resistance to subsolidus alteration (Farver, 2010; Valley, 2003; Valley et al., 1994). In this study we are interested in zircon and garnet that preserve the $\delta^{18}O$ of peraluminous granitic melts. However, not all garnet in peraluminous granites are "magmatic" in that they crystallized from a cooling granitic magma. Instances where garnet forming via peritectic dehydration reaction or as xenocrysts from adjacent metamorphic rocks have been observed in peraluminous granites (Dorais and Campbell, 2022; Erdmann et al., 2009; Harris and Vogeli, 2010; Lackey et al., 2011; Stevens et al., 2007). Whereas xenocyrstic zircon is readily identifiable through U—Pb ages older than the crystallization age of a pluton, identifying xenocrystic (as well as peritectic) garnet requires careful field mapping and textural analysis (Dorais and Campbell, 2022; Lackey et al., 2011). For example, in the South Mountain batholith (Newfoundland), the oxygen isotopes of magmatic, peritectic, and xenocrystic garnet have been shown to exhibit variability in $\delta^{18}O$. At that locality, magmatic and xenocrystic garnet define end-members ~1.3 ‰ apart, with the metamorphic garnet displaying higher $\delta^{18}O$ values. Peritectic garnet falls between the end members, approximately 0.5 ‰ higher than magmatic garnet, suggesting an origin through reactive assimilation of sedimentary host rocks by the granitic magma (Lackey et al., 2011). Furthermore, studies have highlighted that magmatic zircon and garnet in a single granitic pluton can have distinct (and variable) oxygen isotopic values, reflecting evolving magma chemistry due to active assimilation during pluton crystallization (King and Valley, 2001; Quintero et al., 2021).

Most studies included in our compilation lack the detailed investigations of garnet origins. Further, in many cases, either garnet or zircon is analyzed for oxygen isotopes (but not both phases), limiting an evaluation of whether they are in isotopic equilibrium. However, in instances where both zircon and garnet were analyzed from the same sample ($n = 22$ samples), we observe a close correspondence in, with the majority (~7 70 %) exhibiting $\Delta_{garnet\text{-}zircon}$ of ≤1.0 ‰, consistent with small fractionations at magmatic temperatures (Fig. S4a; Valley, 2003; Vho et al., 2019). Moreover, despite quartz having higher rates of oxygen diffusion, in samples where both quartz and garnet were analyzed ($n = 48$) the average fractionation between the phases is 3.3 ± 0.8 ‰ (1σ), consistent with equilibrium fractionation at temperatures typical for granitic magmas (<850 °C, Fig. S4c). This observation supports the assertion that both garnet and quartz broadly preserve magmatic values for the compiled samples. This observation underscores the robustness of oxygen isotope values in zircon, garnet, and to some extent quartz, even in the absence of detailed studies.

Thus, we proceed under the assumption that the oxygen isotopes in zircon and garnet in our compilation are in (or close to) equilibrium with that of the peraluminous granitic melts from which they crystallized. Notably, our analysis relies predominantly on zircon, given its more extensively available data. Intuitively, and substantiated by our modeling, the observed variations in oxygen isotopes are most effectively explained by an increase in the oxygen isotopes of sedimentary source rocks with time. This conclusion is further supported by the similarities between Group 2 and 4, which originated from the melting of sedimentary rocks deposited prior to 600 Ma, despite their distinct crystallization ages (Figs. 3,4). Our model results demonstrate that $\Delta_{melt\text{-}source}$ is <±1 ‰ and that the $\delta^{18}O$ of zircon crystallizing from such melts is ~0.8–2.3 ‰ lower than the source (Fig. 5). Applying a + 0.8–2.3 ‰ correction to our compilation averages (±1 s.d.) indicates that sedimentary source rocks of peraluminous granites on average increased from 6.5 to 10 ‰ to 9.6–12.5 ‰ in the Paleoproterozoic and to 10.5–13.5 ‰ in the Neoproterozoic (Fig. 6). These values are consistent with the lower range of bulk-rock $\delta^{18}O$ values measured for siliciclastic sedimentary rocks (Fig. 6).

4.2. Controls on sedimentary and peraluminous granite oxygen isotopes through time

The $\delta^{18}O$ in siliciclastic sedimentary rocks is controlled by four primary variables: (1) the initial oxygen isotope ratio of the source rock, (2) the ratio of authigenic (secondary) to detrital (primary) minerals, (3) the oxygen isotopic composition of the altering water, and (4) the temperature of fluid-rock interaction (see **Bindeman et al., 2016**; **Bindeman et al., 2018**; **Bindeman, 2021**, for discussion). Here we focus on the first two variables. First, it is generally expected, and demonstrated by analyses of detrital and magmatic zircon (Fig. 1), that the average $\delta^{18}O$ of the continental crust has increased through time due to continual recycling of weathered material. Thus, some increase in $\delta^{18}O$ values of sedimentary rocks is expected. However, the second variable, which combines both the degree of weathering and concentration of weathered minerals, will also have a strong effect. Below we review how these factors may have varied across the temporal transitions observed in the peraluminous granite and siliciclastic sedimentary rock records.

4.2.1. Increase in $\delta^{18}O$ of peraluminous granites from the Archean to Paleoproterozoic

Peraluminous granites derived from melting of sedimentary rocks first appear in the Mesoarchean, but become widespread in the late Neoarchean (**Bucholz and Spencer, 2019**). The source rocks for these granites are thought to be multi-kilometer-thick siliciclastic sedimentary sequences, which were deposited on cratons starting in the late Archean (see review of **Reimink and Smye, 2024**). The development of these sedimentary basins has been linked to the emergence of continents and the onset of subaerial weathering (e.g., **Campbell and Davies, 2017**) and is supported by the diversification of detrital zircon ages in siliciclastic rocks around 2.8 Ga (**Reimink et al., 2021**). These Neoarchean sedimentary deposits represent the first large-scale, preserved reservoir capable of serving as source material for peraluminous granitic melts. The average $\delta^{18}O$ value of zircon from Group 1 peraluminous granites (6.7 ± 1.0, 1 s.d.) aligns with the highest $\delta^{18}O$ values recorded in Archean detrital zircons, which likely reflect the upper limit for magmas derived from weathered sedimentary sources during this period.

Transitioning from the Archean to the Paleoproterozoic, the observed increase in $\delta^{18}O$ values of zircon, garnet, and quartz in peraluminous granites is consistent with studies demonstrating a shift in the $\delta^{18}O$ values of magmatic zircon and garnet from peraluminous granites of the North China Craton (Liebmann et al., 2021a; Lu et al., 2021; Xie et al., 2022), as well as, previous studies of globally distributed peraluminous granites (Bucholz and Spencer, 2019; Liebmann et al., 2021b). Much of the data in our compilation is from these aforementioned studies and as they have noted, the temporal trends in the oxygen isotope record of peraluminous granites broadly align with increases in shale $\delta^{18}O$ (**Bindeman et al., 2016**; **Bindeman et al., 2018**; **Payne et al., 2015**), which represent potential source rocks. However, the shale $\delta^{18}O$ record from the Neoarchean to Paleoproterozoic is limited and exhibits significant scatter (Fig. 1). The simultaneous increase in $\delta^{18}O$

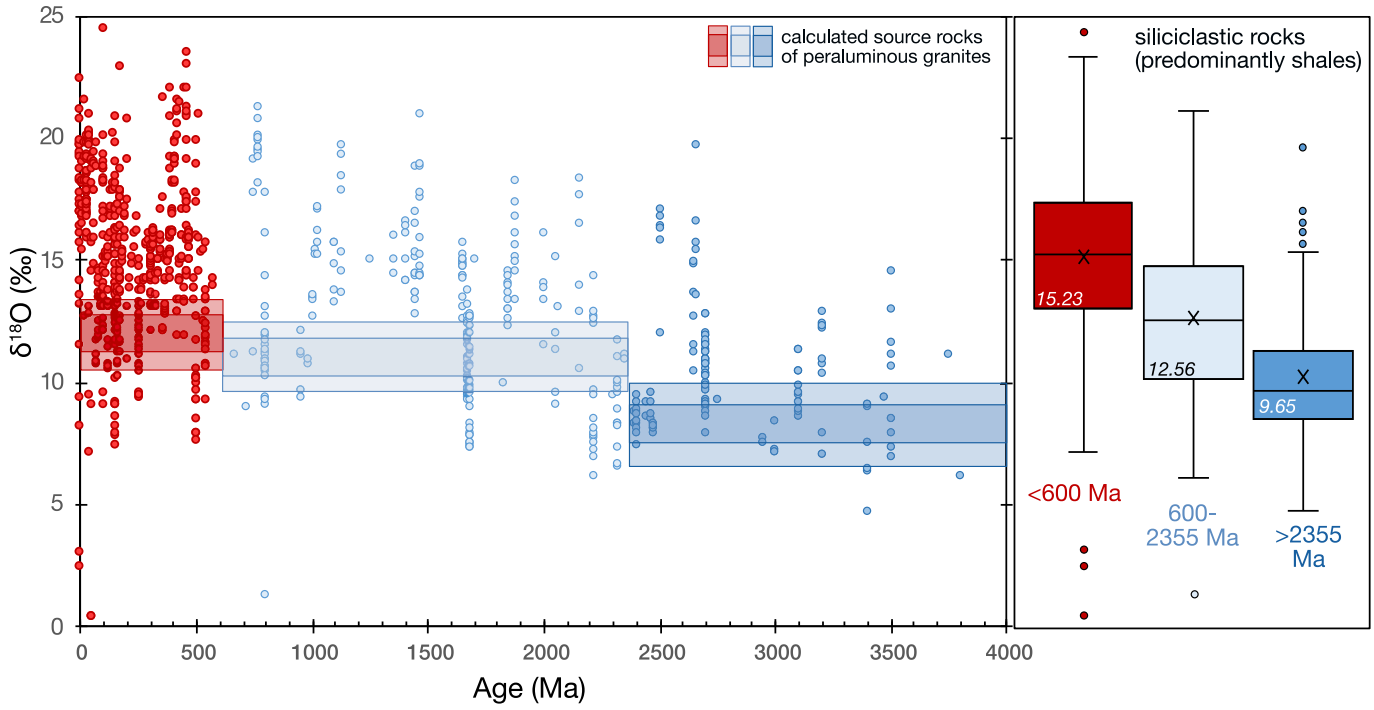

Fig. 6. Oxygen isotopes in siliciclastic sedimentary rocks versus depositional age (data sources as in Fig. 1). Analyses are binned into groups by depositional age (<600 Ma, 600–2355 Ma, >2355 Ma). In the right panel, box and whisker plots with median values of siliciclastic sedimentary rocks indicated by bar (and value in box) and average values indicated by "x". Calculated source rock compositions from peraluminous granites are shown as shaded rectangles in left panel. These calculations are done using the average peraluminous granite zircon $\delta^{18}O$ values (±1 s.d.) and a range of calculated zircon-melt fractionations of 0.8–2.3 ‰.

and decrease in $\Delta^{17}O$ (or per mil fractionation from the $^{17}O/^{16}O$-$^{18}O/^{16}O$ mass fractionation line, see **Bindeman et al., 2018**) of shales has been attributed to widespread emergence of subaerial continents, marking significant shifts in the meteoric water cycle and concurrent reduction in surface temperatures (**Bindeman et al., 2018**). However, this interpretation conflicts with the geologic record, which suggests extensive continental erosion and formation of large sedimentary basins beginning in the Neoarchean, as described above. Continental emergence and increased topographic relief, however, likely continued into the Proterozoic as evidenced by the global stratigraphic and volcanic record indicating an increase in subaerial deposition or eruption at that time (**Eriksson et al., 2005**; **Liebmann et al., 2022**).

As discussed in section 4.2.1, the progressive reworking of crust must also be considered when interpreting the Archean to Proterozoic $\delta^{18}O$ record. For example, the sedimentary source rocks for Paleoproterozoic peraluminous granites were derived from the weathering of Neoarchean continents, which had undergone significant transformation compared to earlier times. By the Neoarchean, crustal composition had shifted away from the dominance of tonalite-trondhjemite-granodiorite (TTG) suites towards a late-stage 'granite bloom' characterized by more potassic and peraluminous granites (Laurent et al., 2014). This period marks a pivotal time in Earth's history, as it represents the first substantial episode of crustal reworking involving weathered material (Reimink and Smye, 2024). If these Neoarchean granites were subsequently eroded and contributed to Paleoproterozoic sedimentary deposits, the sediments derived from them would have inherited their higher $\delta^{18}O$ values. These elevated $\delta^{18}O$ values would then be transferred to the Paleoproterozoic peraluminous granites formed from the melting of Paleoproterozoic sediments, further compounding the increase in $\delta^{18}O$ observed during this time.

Finally, the increase in $\delta^{18}O$ of peraluminous granites in the Paleoproterozoic coincides with the timing of the Great Oxidation Event (Fig. 7b). Notably, sulfur isotopes in peraluminous granites exhibit a concurrent shift with the oxygen isotope record. Before 2.35 Ga peraluminous granites display lower $\delta^{18}O$ values in garnet and zircon, as well as mass-independent fractionation of sulfur isotopes. After 2.35 Ga peraluminous granites are characterized by elevated $\delta^{18}O$ (Fig. 3) and mass dependent fractionation of sulfur isotopes (**Liebmann et al., 2021b**). Although speculative it is possible that the rise of atmospheric oxygen may have also influenced weathering dynamics, expanding the diversity of secondary clay minerals to incorporate Fe^{3+} on both octahedral and tetrahedral sites (**Hazen et al., 2013**). This change in weathering dynamics could have resulted in more clay production, driving Paleoproterozoic siliciclastic sediments to be more clay-rich with higher $\delta^{18}O$ values.

4.2.2. Increase in zircon and garnet $\delta^{18}O$ the Neoproterozoic to Phanerozoic

The peraluminous granite oxygen isotope compilation presented here suggests that on average their sedimentary source rocks increased by ~ 1 ‰ from the Neoproterozoic to the Paleozoic. Unlike the increase in $\delta^{18}O$ values in minerals from peraluminous granites across the Archean-Proterozoic transition, the increase from the Neoproterozoic to Phanerozoic has not been previously documented. This increase, however, is consistent with the multiple lines of evidence from the sedimentary record that from the Neoproterozoic to the Paleozoic terrestrial weathering and clay production and/or deposition was enhanced by various climatic and biological forcings. For example, the sharp increase in $^{87}Sr/^{86}Sr$ ratios of marine carbonates beginning at c. 700 Ma has been attributed to increased feldspar dissolution and release of radiogenic Sr to the oceans during continental weathering (**Shields and Veizer, 2002**; Fig. 7c) potentially related to the orogenesis and enhanced erosion resulting from the amalgamation of Gondwana (**Campbell and Squire, 2010**). Further, there is direct evidence from the sedimentary siliciclastic record. For example, fine-grained clastic sedimentary rocks with depositional ages between 1.7 and 0.2 Ga from the Colorado Plateau display chemical indices of weathering that indicate an increase in the proportion of clay minerals beginning in the Neoproterozoic (**Cox et al., 1995**). An increase in clay mineral content in marine sediments from passive margin sections from three different continents has also been

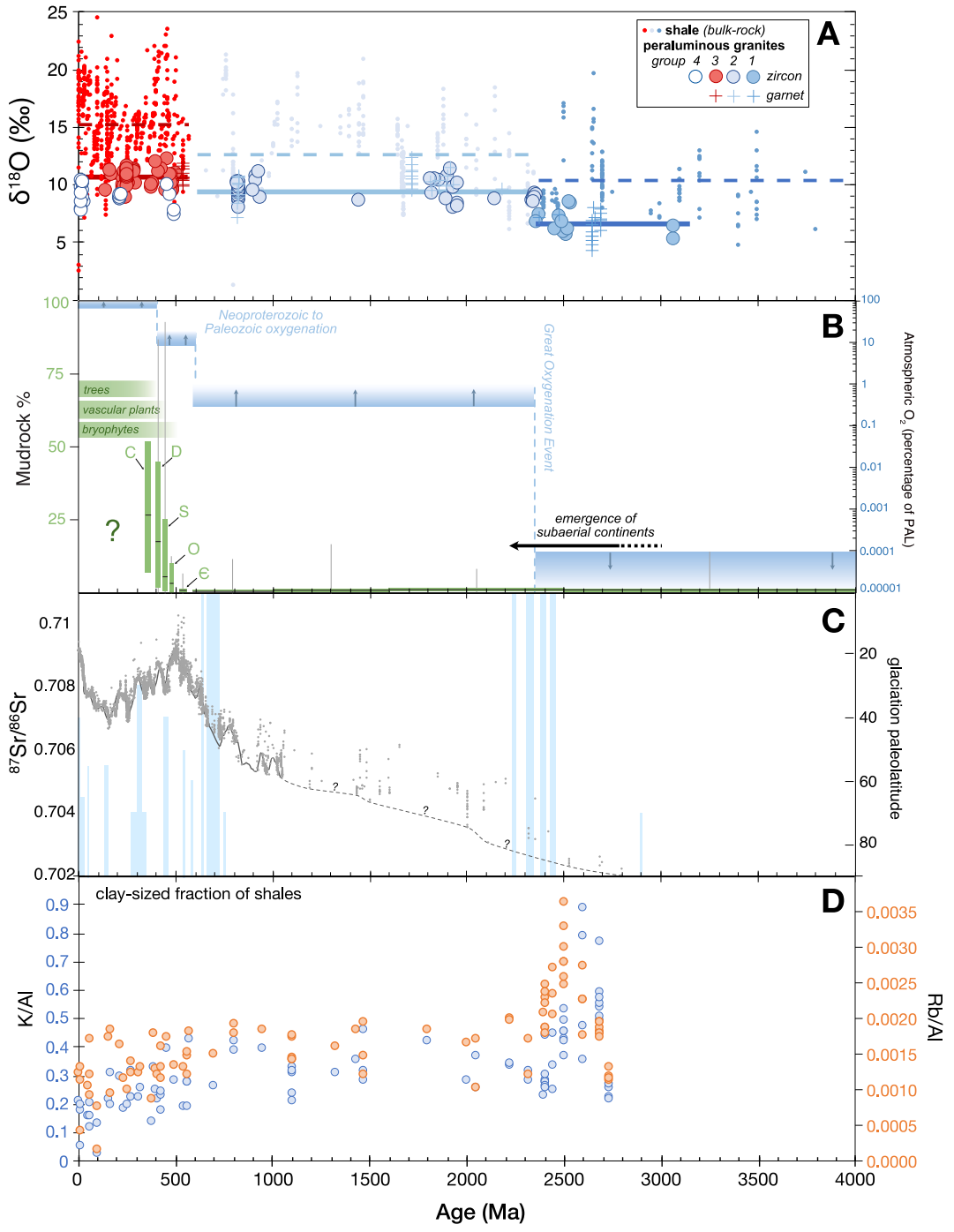

Fig. 7. Summary of oxygen isotope data for peraluminous granites and shales in the context of weathering proxies, Earth oxygenation, and glaciations. (A) $\delta^{18}O$ of shales (as in Fig. 6) and peraluminous granite average zircon and garnet values. Dashed horizontal lines indicate average shale values for >2355 Ma, 600–2355 Ma, and < 600 Ma. Solid horizontal lines indicate the grand mean of $\delta^{18}O$ of zircon for Groups 1, 2, and 3, respectively. (B) Proportion of mudrocks in alluvial sedimentary successions, evolution of terrestrial plants, and history of atmospheric oxygenation. Mudrock box and whisker plots (medians and quartiles) for different geologic ages are from McMahon and Davies (2018). Cambrian (C) and older medians are effectively 0. Beginning in the Ordovician (O) and becoming pronounced in the Silurian (S) and onward (Devonian (D) and Carboniferous (C)) proportions of mudrocks in alluvial succession increase. Mudrock proportions for alluvial succession younger than the Carboniferous were not compiled in that study. Evolution of terrestrial plants is from summary of Fischer (2018). Upper or lower bounds on atmospheric oxygen concentrations are summarized in Catling and Zahnle (2020) (C) Sr isotopes in marine carbonates as compiled in Chen et al. (2022) and history of global glaciations. Black line for data <1000 Ma is interpolation from Chen et al. (2022). For older ages, data is sparse, precluding a well-constrained seawater curve. Dashed line is speculative. Glaciations (shown as vertical blue bars) are from compilation of Walzer and Hendel (2023). (D) K/Al (in blue) and Rb/Al (in orange) of clay-size fraction of shales from Bayon et al. (2022). (For interpretation of the references to colour in this figure legend, the reader is referred to the web version of this article.)

observed beginning in the Neoproterozoic (c. 600 Ma; **Kennedy et al.,** 2006). Additionally, the Rb/Al ratios of clay-size fraction of shales which decrease as K-feldspar weathering progresses due the higher mobility of Rb versus Al during chemical weathering, decrease at c. 0.6 Ga (**Bayon et al.,** 2022; Fig. 7d).

Similarly, the percentage of mudrocks in alluvial (continental) formations increases from being negligible for the first ~ 3.0 billion years of Earth's history to being common to dominant from the Late Ordovician onwards (Fig. 7b; **McMahon and Davies,** 2018). This latter observation has been ascribed to the evolution of land plants (which began at ~ 480 Ma with the first simple bryophytes), which could have simultaneously increased the production of clays particularly when vascular plants evolved in the Devonian (through deepening weathering profiles through rooting, secretion of organic acids, and by developing symbiotic relationships with cyanobacteria and fungi), as well as increased retention of fine sediments in continental deposition through stabilization of sediments in floodplains (**Davies and Gibling,** 2011; **McMahon and Davies,** 2018). Alternatively, this record could be explained by enhanced mud deposition (rather than production) due to greater abundances of organic matter promoting the aggregation of clays into flocs, thus favoring deposition (**Zeichner et al.,** 2021). Although the source rocks of peraluminous granites are deposited in marine settings, enhanced organic matter export to these systems is associated with greater clay deposition due to flocculation of clays with organic matter (**Deng et al.,** 2022).

In sum, multiple lines of evidence from the sedimentary record indicates that weathering and/or clay depositions was enhanced beginning in the Neoproterozoic due to increased weathering in the aftermath of Neoproterozoic global glaciation or the Pan-African Orogeny, that then further accelerated into the Paleozoic with the evolution of land plants. Further, with the final increase in atmospheric oxygen levels to near present-day levels in the Neoproterozoic to Paleozoic (Fig. 7b), oxidative weathering reactions would have further diversified clay mineralogy (**Hazen et al.,** 2013). Our compilation does not have sufficient time resolution to constrain the cause and effect of Earth's oxygenation and enhanced weathering due to the lack of data from between ~550–800 Ma. However, our findings are consistent with a critical role of continental chemical weathering in releasing important macronutrients (e.g, phosphorus) to sustain primary productivity and organic carbon burial in the lead up to the Neoproterozoic oxygenation in Earth's atmosphere (Canfield, 2005).

4.3. Implications for interpreting the zircon $\delta^{18}O$ record and magmatic oxygen isotope values

The progressive increases in $\delta^{18}O$ of calculated source-rocks for peraluminous granites mirror increases observed in the siliciclastic sedimentary record, but only capture the lower $\delta^{18}O$ values of the siliciclastic record (Fig. 6, 7a). This perhaps is not surprising. First, shales define the highest $\delta^{18}O$ endmember of siliciclastic sedimentary rocks due their dominant constituent being clays, as compared to more feldspathic-lithologies such as (grey-)wackes which will have lower $\delta^{18}O$ values. As peraluminous granites are often sourced from marginal marine sedimentary rocks such as turbidites comprised of a mixture of both pelitic and psammitic lithologies (rather than deep sea sediments), it is expected that their source rocks would have a combination of detrital and secondary minerals and their $\delta^{18}O$ values would be on the lower end of the siliciclastic sedimentary rock range (Fig. 6).

Thus, our data compilation and modeling results suggest that sedimentary rocks recycled and incorporated back into magmas (and ultimately the continental crust) have, on average, values lower by ~ 1.5–3 ‰ than the coeval shale average. For analyses of global, time-transgressive data sets of oxygen isotopes in magmatic rocks or detrital zircon, we suggest that it is more appropriate to use the average values of calculated source rocks for peraluminous granites (Fig. 6). Notably, however, this exercise will require caution as older Proterozoic sedimentary rocks have been demonstrably assimilated into Phanerozoic magmas from collisional orogens and arcs (e.g., Hopkinson et al., 2017; Lackey et al., 2008). Alternatively, researchers could look at average $\delta^{18}O$ values for both Group 3 and 4 to quantify the average oxygen isotopic composition of sedimentary rocks being assimilated in the Phanerozoic.

Finally, as our study presents strong evidence for a progressive increase in the $\delta^{18}O$ of siliciclastic sedimentary rocks from the Archean to Proterozoic and finally Phanerozoic, the evolution of this reservoir must be considered in regard to the progressive contamination of the mantle. Mantle-derived basalts have been demonstrated to have $\delta^{18}O$ values elevated above the canonical ~ 5.6 ‰ value due to contamination of the mantle with crustal material during subduction (e.g., Couzinié et al., 2016; see also compilation in **Bucholz et al.,** 2017). The progressive increase in $\delta^{18}O$ of siliciclastic lithologies subducted into the mantle will result in more elevated $\delta^{18}O$ values through time. This in turn would have a feedback mechanism resulting in more and more enriched primary source material which in turn would be weathered, producing sediments with even higher $\delta^{18}O$ (**Cornet et al.,** 2022).

5. Conclusions and future work

Our study provides valuable insights into the evolution of crustal endmembers in magmatic processes, utilizing peraluminous granites as proxies for sedimentary rock recycling throughout Earth's history. Our comprehensive dataset and quantitative modeling of oxygen isotopes fractionation during melting of sedimentary rocks, demonstrate that there is a progressive increase in $\delta^{18}O$ values of zircon and garnet in peraluminous granites from the Archean to the Phanerozoic which is consistent with previously inferred changes in terrestrial weathering. These findings not only align with records from siliciclastic sedimentary rocks but also highlight the complex interplay between tectonic, climatic, and biological factors driving enhanced weathering and clay deposition. Further, our analysis suggests that calculated source-rock $\delta^{18}O$ values capture only the lower end of the siliciclastic sedimentary rock range, indicating that sedimentary rocks recycled into magmas have, on average, lower $\delta^{18}O$ values than coeval shales.

Future work should address temporal gaps in the existing record of oxygen isotopes of peraluminous granites, particularly during the critical periods of 500–800 Ma, the Mesoproterozoic, and the Archean to Proterozoic transition. For example, although increases in the $\delta^{18}O$ values of peraluminous granites are observed across the Archean-Proterozoic transition as well as from the Neoproterozoic to Paleozoic, the lack of temporal resolution in the existing dataset prevents us from understanding whether the increases were sharp or gradational. In addition, triple oxygen isotope analyses may prove fruitful in understanding the environmental and climatic conditions under which their sedimentary source rocks formed, isolating competing effects of temperature variation versus changes in water oxygen isotopic ratios. Although the triple oxygen isotopic variations of magmatic rocks have received less attention, primarily due to the limited fractionation occurring at high temperatures involved in igneous processes, temporal variations in source rock compositions (such as those observed in shales, Bindeman, 2021; Bindeman et al., 2018) should be preserved in magmatic minerals. The variability observed in the sedimentary record and the lack of exploration in the crustal plutonic record raises the distinct possibility that larger variations in triple O isotopes in the igneous rock record exist. Peraluminous granites are a natural archive to first explore this question due to their derivation from sedimentary rocks that have interacted with meteoric waters at low temperatures. SPGs should record the integrated changes in the compositions of the weathered components (e.g., clays) of siliciclastic sedimentary rocks, which in turn can record information about the isotopic composition and temperature of the weathering fluid.

CRediT author statement

Claire Bucholz: Conceptualization, methodology, formal analysis, writing – original draft, review, & editing, visualization, data curation, funding acquisition **Juan Hernández-Montenegro** methodology, modeling, formal analysis, visualization, writing – original draft, review & editing.

CRediT authorship contribution statement

Claire E. Bucholz: Writing – review & editing, Writing – original draft, Visualization, Supervision, Methodology, Investigation, Funding acquisition, Formal analysis, Data curation, Conceptualization. **Juan D. Hernández-Montenegro:** Writing – review & editing, Visualization, Validation, Software, Methodology, Investigation, Formal analysis.

Declaration of competing interest

The authors declare that they have no known competing financial interests or personal relationships that could have appeared to influence the work reported in this paper.

Acknowledgements

This work was supported by NSF grant EAR-1943629. Juan David Hernández-Montenegro acknowledges support by Fulbright Colombia. We thank Jesse Reimink, John Valley, and one anonymous reviewer for their thoughtful comments that helped strengthen this paper.

Appendix A. Supplementary data

Supplementary data to this article can be found online at https://doi.org/10.1016/j.lithos.2024.107864.

References

Bayon, G., Bindeman, I.N., Trinquier, A., Retallack, G.J., Bekker, A., 2022. Long-term evolution of terrestrial weathering and its link to Earth's oxygenation. Earth Planet. Sci. Lett. 584, 117490. https://doi.org/10.1016/j.epsl.2022.117490.

Bindeman, I.N., 2021. Triple Oxygen Isotopes in Evolving Continental Crust, Granites, and Clastic Sediments. Rev. Mineral. Geochem. 86, 241–290.

Bindeman, I.N., Bekker, A., Zakharov, D.O., 2016. Oxygen isotope perspective on crustal evolution on early Earth: a record of Precambrian shales with emphasis on Paleoproterozoic glaciations and Great Oxygenation Event. Earth Planet. Sci. Lett. 437, 101–113. https://doi.org/10.1016/j.epsl.2015.12.029.

Bindeman, I.N., Zakharov, D.O., Palandri, J., Greber, N.D., Dauphas, N., Retallack, G.J., Hofmann, A., Lackey, J.S., Bekker, A., 2018. Rapid emergence of subaerial landmasses and onset of a modern hydrologic cycle 2.5 billion years ago. Nature 557, 545–548. https://doi.org/10.1038/s41586-018-0131-1.

Bonin, B., Janoušek, V., Moyen, J.-F., 2020. Chemical variation, modal composition and classification of granitoids. Geol. Soc. Lond. Spec. Publ. 491, 9–51.

Bucholz, C.E., 2022. Coevolution of sedimentary and strongly peraluminous granite phosphorus records. Earth and Planetary Science Letters 596, 117795.

Bucholz, C.E., 2025. The Diversity and Origin of Granites, in: Treatise in Geochemistry. Elsevier, UK, pp. 153–202. https://doi.org/10.1016/B978-0-323-99762-1.00006-1.

Bucholz, C.E., Spencer, C.J., 2019. Strongly Peraluminous Granites across the Archean–Proterozoic Transition. J. Petrol. 60, 1299–1348. https://doi.org/10.1093/petrology/egz033.

Bucholz, C.E., Jagoutz, O., VanTongeren, J.A., Setera, J., Wang, Z., 2017. Oxygen isotope trajectories of crystallizing melts: Insights from modeling and the plutonic record. Geochim. Cosmochim. Acta 207, 154–184. https://doi.org/10.1016/j.gca.2017.03.027.

Bucholz, C.E., Stolper, E.M., Eiler, J.M., Breaks, F.W., 2018. A comparison of oxygen fugacities of strongly peraluminous granites across the Archean–Proterozoic Boundary. J. Petrol. 59, 2123–2156. https://doi.org/10.1093/petrology/egy091.

Bucholz, C.E., Liebmann, J., Spencer, C.J., 2022. Secular variability in zircon phosphorus concentrations prevents simple petrogenetic classification. Geochem. Persp. Let. 24, 12–16. https://doi.org/10.7185/geochemlet.2240.

Campbell, I.H., Davies, D.R., 2017. Raising the continental crust. Earth Planet. Sci. Lett. 460, 112–122. https://doi.org/10.1016/j.epsl.2016.12.011.

Campbell, I.H., Squire, R.J., 2010. The mountains that triggered the late Neoproterozoic increase in oxygen: the Second Great Oxidation Event. Geochim. Cosmochim. Acta 74, 4187–4206. https://doi.org/10.1016/j.gca.2010.04.064.

Canfield, D.E., 2005. The early history of Atmospheric Oxygen: Homage to Robert M. Garrels. Annu. Rev. Earth Planet. Sci. 33, 1–36. https://doi.org/10.1146/annurev.earth.33.092203.122711.

Catling, D.C., Zahnle, K.J., 2020. The Archean atmosphere. Sci. Adv. 6, eaax1420. https://doi.org/10.1126/sciadv.aax1420.

Cavosie, A.J., Kita, N.T., Valley, J.W., 2009. Primitive oxygen-isotope ratio recorded in magmatic zircon from the Mid-Atlantic Ridge. Am. Mineral. 94, 926–934. https://doi.org/10.2138/am.2009.2982.

Chappell, B.W., White, A.J.R., 1974. Two contrasting granite types. Pac. Geol. 8, 173–174.

Chen, X., Zhou, Y., Shields, G.A., 2022. Progress towards an improved Precambrian seawater $^{87}Sr/^{86}Sr$ curve. Earth Sci. Rev. 224, 103869. https://doi.org/10.1016/j.earscirev.2021.103869.

Clayton, R.N., Mayeda, T.K., 1963. The use of bromine pentafluoride in the extraction of oxygen from oxides and silicates for isotopic analysis. Geochim. Cosmochim. Acta 27, 43–52. https://doi.org/10.1016/0016-7037(63)90071-1.

Cleveland, W.S., 1979. Robust locally Weighted Regression and Smoothing Scatterplots. J. Am. Stat. Assoc. 74, 829–836.

Cornet, J., Laurent, O., Wotzlaw, J.-F., Antonelli, M.A., Otamendi, J., Bergantz, G.W., Bachmann, O., 2022. Reworking subducted sediments in arc magmas and the isotopic diversity of the continental crust: the case of the Ordovician Famatinian crustal section, Argentina. Earth Planet. Sci. Lett. 595, 117706. https://doi.org/10.1016/j.epsl.2022.117706.

Couzinié, S., Laurent, O., Moyen, J.-F., Zeh, A., Bouilhol, P., Villaros, A., 2016. Post-collisional magmatism: Crustal growth not identified by zircon Hf–O isotopes. Earth Planet. Sci. Lett. 456, 182–195. https://doi.org/10.1016/j.epsl.2016.09.033.

Cox, R., Lowe, D.R., Cullers, R.L., 1995. The influence of sediment recycling and basement composition on evolution of mudrock chemistry in the southwestern United States. Geochim. Cosmochim. Acta 59, 2919–2940. https://doi.org/10.1016/0016-7037(95)00185-9.

Davies, N.S., Gibling, M.R., 2011. Evolution of fixed-channel alluvial plains in response to Carboniferous vegetation. Nat. Geosci. 4, 629–633. https://doi.org/10.1038/ngeo1237.

Deng, Z., Huang, D., He, Q., Chassagne, C., 2022. Review of the action of organic matter on mineral sediment flocculation. Front. Earth Sci. 10, 965919. https://doi.org/10.3389/feart.2022.965919.

Dorais, M.J., Campbell, S., 2022. Peritectic and phenocrystic garnet accumulation and the origin of strongly peraluminous granitic rocks: the Flagstaff Lake Igneous complex, Maine. Lithos 418–419, 106680. https://doi.org/10.1016/j.lithos.2022.106680.

Eiler, J.M., 2001. Oxygen isotope variations of basaltic lavas and upper mantle rocks. Rev. Mineral. Geochem. 43, 319–364.

Eiler, J.M., Graham, C., Valley, J.W., 1997. SIMS analysis of oxygen isotopes: matrix effects in complex minerals and glasses. Chem. Geol. 138, 221–244. https://doi.org/10.1016/S0009-2541(97)00015-6.

Eiler, J.M., Schiano, P., Kitchen, N., Stolper, E.M., 2000. Oxygen-isotope evidence for recycled crust in the sources of mid-ocean-ridge basalts. Nature 403, 530–534. https://doi.org/10.1038/35000553.

Erdmann, S., Jamieson, R.A., MacDonald, M.A., 2009. Evaluating the Origin of Garnet, Cordierite, and Biotite in Granitic Rocks: a Case Study from the South Mountain Batholith, Nova Scotia. J. Petrol. 50, 1477–1503. https://doi.org/10.1093/petrology/egp038.

Eriksson, P.G., Catuneanu, O., Sarkar, S., Tirsgaard, H., 2005. Patterns of sedimentation in the Precambrian. Sediment. Geol. 176, 17–42. https://doi.org/10.1016/j.sedgeo.2005.01.003.

Farver, J.R., 2010. Oxygen and Hydrogen Diffusion in Minerals. Rev. Mineral. Geochem. 72, 447–507. https://doi.org/10.2138/rmg.2010.72.10.

Fischer, W.W., 2018. Early plants and the rise of mud. Science 359, 994–995. https://doi.org/10.1126/science.aas9886.

Forshaw, J.B., Pattison, D.R.M., 2023. Major-element geochemistry of pelites. Geology 51, 39–43. https://doi.org/10.1130/G50542.1.

Gao, P., Zhao, Z.-F., Zheng, Y.-F., 2014. Petrogenesis of Triassic granites from the Nanling Range in South China: Implications for geochemical diversity in granites. Lithos 210–211, 40–56. https://doi.org/10.1016/j.lithos.2014.09.027.

Grimes, C.B., Wooden, J.L., Cheadle, M.J., John, B.E., 2015. "Fingerprinting" tectono-magmatic provenance using trace elements in igneous zircon. Contrib. Mineral. Petrol. 170, 46. https://doi.org/10.1007/s00410-015-1199-3.

Harris, C., Vogeli, J., 2010. Oxygen Isotope Composition of Garnet in the Peninsula Granite, Cape Granite Suite, South Africa: Constraints on Melting and Emplacement Mechanisms. S. Afr. J. Geol. 113, 401–412. https://doi.org/10.2113/gssajg.113.4.401.

Hazen, R.M., Sverjensky, D.A., Azzolini, D., Bish, D.L., Elmore, S.C., Hinnov, L., Milliken, R.E., 2013. Clay mineral evolution. Am. Mineral. 98, 2007–2029. https://doi.org/10.2138/am.2013.4425.

Holder, R.M., Viete, D.R., Brown, M., Johnson, T.E., 2019. Metamorphism and the evolution of plate tectonics. Nature 572, 378–381. https://doi.org/10.1038/s41586-019-1462-2.

Holland, T., Powell, R., 2003. Activity-composition relations for phases in petrological calculations: an asymmetric multicomponent formulation. Contrib. Mineral. Petrol. 145, 492–501. https://doi.org/10.1007/s00410-003-0464-z.

Holland, T.J.B., Powell, R., 2011. An improved and extended internally consistent thermodynamic dataset for phases of petrological interest, involving a new equation of state for solids. J. Metamorph. Geol. 29, 333–383. https://doi.org/10.1111/j.1525-1314.2010.00923.x.

Hopkinson, T.N., Harris, N.B.W., Warren, C.J., Spencer, C.J., Roberts, N.M.W., Horstwood, M.S.A., Parrish, R.R., Eimf, 2017. The identification and significance of

pure sediment-derived granites. Earth Planet. Sci. Lett. 467, 57–63. https://doi.org/10.1016/j.epsl.2017.03.018.
Husson, J.M., Peters, S.E., 2017. Atmospheric oxygenation driven by unsteady growth of the continental sedimentary reservoir. Earth Planet. Sci. Lett. 460, 68–75. https://doi.org/10.1016/j.epsl.2016.12.012.
Kennedy, M., Droser, M., Mayer, L.M., Pevear, D., Mrofka, D., 2006. Late Precambrian Oxygenation; Inception of the Clay Mineral Factory. Science 311, 1446–1449. https://doi.org/10.1126/science.1118929.
King, E.M., Valley, J.W., 2001. The source, magmatic contamination, and alteration of the Idaho batholith. Contrib. Mineral. Petrol. 142, 72–88. https://doi.org/10.1007/s004100100278.
Kita, N.T., Ushikubo, T., Fu, B., Valley, J.W., 2009. High precision SIMS oxygen isotope analysis and the effect of sample topography. Chem. Geol. 264, 43–57. https://doi.org/10.1016/j.chemgeo.2009.02.012.
Kita, N.T., Huberty, J.M., Kozdon, R., Beard, B.L., Valley, J.W., 2011. High-precision SIMS oxygen, sulfur and iron stable isotope analyses of geological materials: accuracy, surface topography and crystal orientation. Surf. Interface Anal. 43, 427–431. https://doi.org/10.1002/sia.3424.
Kress, V.C., Carmichael, I.S.E., 1991. The compressibility of silicate liquids containing Fe_2O_3 and the effect of composition, temperature, oxygen fugacity, and pressure on their redox states. Contrib. Mineral. Petrol. 108, 82–92.
Lackey, J.S., Valley, J.W., Chen, J.H., Stockli, D.F., 2008. Dynamic Magma Systems, Crustal Recycling, and Alteration in the Central Sierra Nevada Batholith: the Oxygen Isotope Record. J. Petrol. 49, 1397–1426. https://doi.org/10.1093/petrology/egn030.
Lackey, J.S., Erdmann, S., Hark, J.S., Nowak, R.M., Murray, K.E., Clarke, D.B., Valley, J.W., 2011. Tracing Garnet Origins in Granitoid Rocks by Oxygen Isotope Analysis: examples from the South Mountain Batholith, Nova Scotia. Can. Mineral. 49, 417–439. https://doi.org/10.3749/canmin.49.2.417.
Laurent, O., Martin, H., Moyen, J.F., Doucelance, R., 2014. The diversity and evolution of late-Archean granitoids: evidence for the onset of "modern-style" plate tectonics between 3.0 and 2.5Ga. Lithos 205, 208–235. https://doi.org/10.1016/j.lithos.2014.06.012.
Liebmann, J., Spencer, C.J., Kirkland, C.L., Bucholz, C., He, X., Santosh, M., Xia, X.P., Martin, L., Evans, N.J., 2021a. Emergence of continents above sea-level influences sediment melt composition. Terra Nova 33, 465–474. https://doi.org/10.1111/ter.12531.
Liebmann, J., Spencer, C.J., Kirkland, C.L., Bucholz, C.E., Xia, X.-P., Martin, L., Kitchen, N., Shumlyanskyy, L., 2021b. Coupling sulfur and oxygen isotope ratios in sediment melts across the Archean-Proterozoic transition. Geochim. Cosmochim. Acta 307, 242–257. https://doi.org/10.1016/j.gca.2021.05.045.
Liebmann, J., Spencer, C.J., Kirkland, C.L., Xia, X.-P., Bourdet, J., 2021c. Effect of water on $\delta^{18}O$ in zircon. Chem. Geol. 574, 120243. https://doi.org/10.1016/j.chemgeo.2021.120243.
Liebmann, J., Spencer, C.J., Kirkland, C.L., Ernst, R.E., 2022. Large igneous provinces track fluctuations in subaerial exposure of continents across the Archean-Proterozoic transition. Terra Nova 34, 323–329. https://doi.org/10.1111/ter.12594.
Liebmann, J., Kirkland, C.L., Cliff, J.B., Spencer, C.J., Cavosie, A.J., 2023. Strategies towards robust interpretations of in situ zircon oxygen isotopes. Geosci. Front. 14, 101523. https://doi.org/10.1016/j.gsf.2022.101523.
Lu, G., Spencer, C.J., Tian, Y., Wang, W., 2021. Significant increase of Continental Freeboard during the early Paleoproterozoic: Insights from Metasediment-Derived Granites. Geophys. Res. Lett. 48. https://doi.org/10.1029/2021GL096049.
McMahon, W.J., Davies, N.S., 2018. Evolution of alluvial mudrock forced by early land plants. Science 359, 1022–1024. https://doi.org/10.1126/science.aan4660.
Mojzsis, S.J., Harrison, T.M., Pidgeon, R.T., 2001. Oxygen-isotope evidence from ancient zircons for liquid water at the Earth's surface 4,300 Myr ago. Nature 409, 178–181. https://doi.org/10.1038/35051557.
O'Neil, J.R., Chappell, B.W., 1977. Oxygen and hydrogen isotope relations in the Berridale batholith. JGS 133, 559–571. https://doi.org/10.1144/gsjgs.133.6.0559.
O'Neil, J.R., Shaw, S.E., Flood, R.H., 1977. Oxygen and hydrogen isotope compositions as indicators of granite genesis in the New England Batholith, Australia. Contrib. Mineral. Petrol. 62, 313–328. https://doi.org/10.1007/BF00371018.
Page, F.Z., Fu, B., Kita, N.T., Fournelle, J., Spicuzza, M.J., Schulze, D.J., Viljoen, F., Basei, M.A.S., Valley, J.W., 2007. Zircons from kimberlite: New insights from oxygen isotopes, trace elements, and Ti in zircon thermometry. Geochim. Cosmochim. Acta 71, 3887–3903. https://doi.org/10.1016/j.gca.2007.04.031.
Payne, J.L., Hand, M., Pearson, N.J., Barovich, K.M., McInerney, D.J., 2015. Crustal thickening and clay: Controls on O isotope variation in global magmatism and siliciclastic sedimentary rocks. Earth Planet. Sci. Lett. 412, 70–76. https://doi.org/10.1016/j.epsl.2014.12.037.
Pidgeon, R.T., Nemchin, A.A., Whitehouse, M.J., 2017. The effect of weathering on U–Th–Pb and oxygen isotope systems of ancient zircons from the Jack Hills, Western Australia. Geochim. Cosmochim. Acta 197, 142–166. https://doi.org/10.1016/j.gca.2016.10.005.
Quintero, R.R., Kitajima, K., Lackey, J.S., Kozdon, R., Strickland, A., Valley, J.W., 2021. Oxygen isotope ratios in zircon and garnet: a record of assimilation and fractional crystallization in the Dinkey Dome peraluminous granite, Sierra Nevada, California. Am. Mineral. 106, 715–729. https://doi.org/10.2138/am-2021-7472.
Reimink, J.R., Smye, A.J., 2024. Subaerial weathering drove stabilization of continents. Nature 629, 609–615. https://doi.org/10.1038/s41586-024-07307-1.
Reimink, J.R., Davies, J.H.F.L., Ielpi, A., 2021. Global zircon analysis records a gradual rise of continental crust throughout the Neoarchean. Earth Planet. Sci. Lett. 554, 116654. https://doi.org/10.1016/j.epsl.2020.116654.
Roberts, N.M.W., Yakymchuk, C., Spencer, C.J., Keller, C.B., Tapster, S.R., 2024. Revisiting the discrimination and distribution of S-type granites from zircon trace element composition. Earth Planet. Sci. Lett. 633, 118638. https://doi.org/10.1016/j.epsl.2024.118638.
Sharp, Z.D., 1990. A laser-based microanalytical method for the in situ determination of oxygen isotope ratios of silicates and oxides. Geochim. Cosmochim. Acta 54, 1353–1357. https://doi.org/10.1016/0016-7037(90)90160-M.
Shields, G., Veizer, J., 2002. Precambrian marine carbonate isotope database: Version 1.1. Geochem. Geophys. Geosyst. 3. https://doi.org/10.1029/2001GC000266.
Spencer, C.J., Cavosie, A.J., Raub, T.D., Rollinson, H., Jeon, H., Searle, M.P., Miller, J.A., McDonald, B.J., Evans, N.J., 2017. Edinburgh Ion Microprobe Facility (EIMF), Evidence for melting mud in Earth's mantle from extreme oxygen isotope signatures in zircon. Geology 45 (11), 975–978.
Spencer, C.J., Partin, C.A., Kirkland, C.L., Raub, T.D., Liebmann, J., Stern, R.A., 2019. Paleoproterozoic increase in zircon $\delta^{18}O$ driven by rapid emergence of continental crust. Geochim. Cosmochim. Acta 257, 16–25. https://doi.org/10.1016/j.gca.2019.04.016.
Spencer, C.J., Cavosie, A.J., Morrell, T.R., Lu, G.M., Liebmann, J., Roberts, N.M.W., 2022. Disparities in oxygen isotopes of detrital and igneous zircon identify erosional bias in crustal rock record. Earth Planet. Sci. Lett. 577, 117248. https://doi.org/10.1016/j.epsl.2021.117248.
Stevens, G., Villaros, A., Moyen, J.-F., 2007. Selective peritectic garnet entrainment as the origin of geochemical diversity in S-type granites. Geol 35, 9. https://doi.org/10.1130/G22959A.1.
Sundell, K.E., Macdonald, F.A., Puetz, S.J., 2024. Does zircon geochemistry record global sediment subduction? Geology 52, 282–286. https://doi.org/10.1130/G51817.1.
Taylor, H.P., 1968. The oxygen isotope geochemistry of igneous rocks. Contrib. Mineral. Petrol. 19, 1–71. https://doi.org/10.1007/BF00371729.
Valley, J.W., 2003. Oxygen Isotopes in Zircon. Rev. Mineral. Geochem. 53, 343–385.
Valley, J.W., Graham, C.M., 1991. Ion microprobe analysis of oxygen isotope ratios in granulite facies magnetites: diffusive exchange as a guide to cooling history. Contrib. Mineral. Petrol. 109, 38–52. https://doi.org/10.1007/BF00687199.
Valley, J.W., Chiarenzelli, J.R., McLelland, J.M., 1994. Oxygen isotope geochemistry of zircon. Earth Planet. Sci. Lett. 126, 187–206. https://doi.org/10.1016/0012-821X(94)90106-6.
Valley, J.W., Lackey, J.S., Cavosie, A.J., Clechenko, C.C., Spicuzza, M.J., Basei, M.A.S., Bindeman, I.N., Ferreira, V.P., Sial, A.N., King, E.M., Peck, W.H., Sinha, A.K., Wei, C.S., 2005. 4.4 billion years of crustal maturation: oxygen isotope ratios of magmatic zircon. Contrib. Mineral. Petrol. 150, 561–580. https://doi.org/10.1007/s00410-005-0025-8.
Vho, A., Lanari, P., Rubatto, D., 2019. An Internally-Consistent Database for Oxygen Isotope Fractionation between Minerals. J. Petrol. 60, 2101–2129. https://doi.org/10.1093/petrology/egaa001.
Walzer, U., Hendel, R., 2023. Natural climate change and glaciations. Earth Sci. Rev. 241, 104435. https://doi.org/10.1016/j.earscirev.2023.104435.
Wang, X.-L., Coble, M.A., Valley, J.W., Shu, X.-J., Kitajima, K., Spicuzza, M.J., Sun, T., 2014. Influence of radiation damage on Late Jurassic zircon from southern China: Evidence from in situ measurements of oxygen isotopes, laser Raman, U–Pb ages, and trace elements. Chem. Geol. 389, 122–136. https://doi.org/10.1016/j.chemgeo.2014.09.013.
Warr, L.N., 2021. IMA–CNMNC approved mineral symbols. MinMag 85, 291–320. https://doi.org/10.1180/mgm.2021.43.
Whalen, J.B., Chappell, B.W., 1988. Opaque mineralogy and mafic mineral chemistry of I- and S-type granites of the Lachlan fold belt, Southeast Australia. Am. Mineral. 73, 281–296.
White, R.W., Powell, R., Clarke, G.L., 2002. The interpretation of reaction textures in Fe-rich metapelitic granulites of the Musgrave Block, Central Australia: constraints from mineral equilibria calculations in the system K_2O–FeO–MgO–Al_2O_3–SiO_2–H_2O–TiO_2–Fe_2O_3. J. Metamorph. Geol. 20, 41–55. https://doi.org/10.1046/j.0263-4929.2001.00349.x.
White, R.W., Powell, R., Holland, T.J.B., Johnson, T.E., Green, E.C.R., 2014a. New mineral activity–composition relations for thermodynamic calculations in metapelitic systems. J. Metamorph. Geol. 32, 261–286. https://doi.org/10.1111/jmg.12071.
White, R.W., Powell, R., Holland, T.J.B., Worley, n.d. B.A.,2000. The effect of TiO_2 and Fe_2O_3 on metapelitic assemblages at greenschist and amphibolite facies conditions: mineral equilibria calculations in the system K_2O–FeO–MgO–Al_2O_3–SiO$_2$–H_2O–TiO_2–Fe_2O_3. J. Metamorph. Geol. 18, 497–511. doi:10.1046/j.1525-1314.2000.00269.x.
White, R.W., Powell, R., Johnson, T.E., 2014b. The effect of Mn on mineral stability in metapelites revisited: new $a - x$ relations for manganese-bearing minerals. J. Metamorph. Geol. 32, 809–828. https://doi.org/10.1111/jmg.12095.
Wilde, S.A., Valley, J.W., Peck, W.H., Graham, C.M., 2001. Evidence from detrital zircons for the existence of continental crust and oceans on the Earth 4.4 Gyr ago. Nature 409, 175–178. https://doi.org/10.1038/35051550.
Wu, R.-X., Zheng, Y.-F., Wu, Y.-B., Zhao, Z.-F., Zhang, S.-B., Liu, X., Wu, F.-Y., 2006. Reworking of juvenile crust: Element and isotope evidence from Neoproterozoic granodiorite in South China. Precambrian Res. 146, 179–212. https://doi.org/10.1016/j.precamres.2006.01.012.
Xie, S.-W., Wang, F., Bucholz, C.E., Liu, F.-L., Wang, P.-Z., Bao, Z.-M., Liu, D.-Y., 2022. Whole-rock geochemistry and zircon O-Hf isotope compositions of ca. 2.35 Ga strongly peraluminous granites: Implications for increase in zircon $\delta^{18}O$ values during the Paleoproterozoic. Geochim. Cosmochim. Acta 332, 186–202. https://doi.org/10.1016/j.gca.2022.06.029.
Zeichner, S.S., Nghiem, J., Lamb, M.P., Takashima, N., De Leeuw, J., Ganti, V., Fischer, W.W., 2021. Early plant organics increased global terrestrial mud deposition through enhanced flocculation. Science 371, 526–529. https://doi.org/10.1126/science.abd0379.